State-of-charge estimation of power lithium-ion batteries based on an embedded micro control unit using a square root cubature Kalman filter at various ambient temperatures

X. Y. Cui[a], Z. C. He[a*], Eric Li[b*], A. G. Cheng[a], M. J. Luo[c], Y. Z. Guo[c]

[a]State Key Laboratory of Advanced Design and Manufacturing for Vehicle Body, Hunan University, Changsha, 410082 P. R. China

[b]School of Science, Engineering & Design, Teesside University, Middlesbrough, UK

[c]Hubei Key Laboratory of Advanced Technology for Automotive Components, Wuhan University of Technology, Wuhan, 430070, P. R. China

***Corresponding authors**

Tel./Fax: +86 73188822051

E-mail: hezhicheng815@hnu.edu.cn

E-mail: ericsg2012@gmail.com

Summary

The development of a novel method to estimate the state of charge (SOC) with low read-only memory (ROM) occupancy, high stability and high anti-interference capability is very important for the battery management system (BMS) in actual electric vehicles. This paper proposes the square root cubature Kalman filter (SRCKF) with a temperature correction rule, based on the BMS of a common on-board embedded micro control unit (MCU), to achieve smooth estimation of SOC. The temperature correction rule is able to reduce the testing effort and ROM space used for data table storage (189.3 kilobytes is much smaller than the storage of the MPC5604B, with 1000 kilobytes), while the SRCKF is adopted to achieve highly robust real-time SOC estimation with high resistance to interference and moderate computing cost (68.3% of the load rate of the MPC5604B). The results of multiple experiments show that the proposed method with less computational complexity converges rapidly (in approximately 2.5 s) and estimates the SOC of the battery accurately under dynamic temperature condition. Moreover, the SRCKF algorithm is not sensitive to the high measuring interference and highly nonlinear working conditions (even with 1% current and voltage measurement disturbances, the root mean square error of the proposed method can be as high as 0.679%).

Keywords: square root cubature Kalman filter, embedded micro control unit, lithium-ion battery, temperature correction rules, state of charge, electric vehicles

1 Introduction

The lithium-ion battery (LIB) enjoys the merits of a longer cycle life and higher energy density and thus has been widely used in electric vehicles.[1-4] While continuous efforts have been made towards cell optimization,[5-8] the safe and efficient operation of LIB systems still relies on well-designed BMSs that accurately estimate and adjust the SOC. In spite of its importance, the SOC estimation based on an embedded MCU is still challenging due to the high computing cost and storage occupancy of most estimation algorithms.

The most widely used method of SOC estimation in electric vehicles is coulomb counting (CC).[9] However, the CC method requires the initial SOC value in advance. Therefore, the error becomes larger in SOC estimation if there is an error in the initial SOC value. The CC method also has poor anti-interference performance. Although computational intelligence methods such as the neural network (NN)[10] can well approximate a highly nonlinear system with multiple variables, a large amount of read-only memory (ROM) is needed to store the training data, which bars their application, the support vector machine (SVM)[11] is also a computational intelligence methods. The proportional-integral observer (PIO)[12] can realize relatively accurate SOC estimation with limited computing cost while maintaining a high robustness in the presence of model uncertainty. However, the unsuitable design of the controller may lead to inaccurate results.

The define RT-filter is the mainstream for real-time SOC estimation. A classical method for nonlinear system observation is the extended Kalman filter (EKF),[13] but it may suffer from low accuracy or even divergence for highly nonlinear conditions due to the use of the first-order

Taylor expansion. In contrast, the unscented Kalman filter (UKF)[14] uses a third-order Taylor expansion that enhances the SOC estimation precision but at the outlay of higher computing cost. A particle filter (PF)[15] can maintain high robustness and estimation accuracy under strongly nonlinear conditions. However, the requirements for a large number of offline experiments and good processing machine for data processing prohibit its actual application, especially when high measurement interferences are present. The H-infinity filter[16] can achieve higher estimation accuracy and faster convergence with less calculation effort, but the uncertainties caused by dynamic temperature and ageing compromise its performance. The recursive least squares (RLS) method can well address the uncertainties from dynamic working conditions by online adapting of model parameters so that the offline testing effort largely can be reduced, and the conjunction of RLS with suitable observers has been shown to further provide accurate SOC estimation.[17-19] However, the RLS provides biased identification in the case of strong measurement interference.[20] In this regard, to address the noise effect a bias-compensating method which is based on recursive total least squares[21] has been proposed. Using this method, an improved accuracy on identification of model and state estimation has been achieved. But in other hand, the sufficient external excitation is required by such regression methods; thus, their application for the charging process is challenging. Compared to the UKF, the cubature Kalman filter (CKF)[22] adopts the third-order Taylor expansion for nonlinear approximation with much lower computing complexity. However, divergence still occurs under strongly nonlinear conditions. Although the bi-linear interpolation (Bi)[23] has a high accuracy and robustness, it requires a 3D look-up table that occupies a large amount of ROM and limits their application on an embedded

MCU. Zou et al. proposed the fractional-order observer[24] for SOC estimation of lithium-ion batteries, but the fractional-order method generally leads to large computational cost which is unfavourable for embedded MCU on vehicles.

On the other hand, temperature has a great influence on battery capacity and other measures of performance.[25,26] For example, the battery capacity decreases up to 20% in the low temperature area.[27-29] To accurately describe the relationship between battery parameters and temperature, Liu et al.[30] proposed a battery model with temperature compensation. The accuracy reduction caused by the temperature change can be theoretically addressed by such models but at higher computing cost. In addition, temperature is considered the input variable of the model, and at different temperatures, the fine difference of the open circuit voltage (OCV) curve is considered at $0.3<SOC<0.8$.[31] In this way, the SOC estimation accuracy is largely improved. However, the errors in other SOC ranges are still large.

Although many endeavours have been made in real-time SOC estimation, some problems still remain to be solved to meet the application requirements of actual car BMSs based on embedded MCUs. For the actual application of a BMS, the following requirements for SOC estimation must be satisfied. (1) The algorithm cannot be too complex. A certain amount of computing resources should be allocated to other BMS issues which limits the use of complex algorithms for SOC estimation. (2) SOC estimation must be adaptive in real time with higher robustness, faster convergence, higher precision, and greater resistance to measurement interference under strong nonlinear working conditions. (3) The ROM of the embedded MCU for storing data is limited, and the size of a data lookup table is also strictly limited.

To realize real-time battery SOC estimation using the on-board embedded MCU, a novel method combining SRCKF with temperature correction rules, is proposed in this work. To be specific, this method uses the first-order resistance-capacitance (RC) model with parameters identified offline via innovative temperature correction rules so that the number of hybrid pulse power characteristic (HPPC) tests and the ROM needed for the data table can substantially be reduced. Based on the obtained model, the SRCKF algorithm, which manifests itself with high robustness and anti-interference, is proposed for real-time SOC estimation in the embedded MCU environment. The algorithm is verified by the results of multiple experiments such that the method proposed in this paper estimates the SOC accurately with rapid convergence and high stability under high measurement interference and highly nonlinear conditions. The use of the proposed method in an actual BMS environment further verifies its feasibility and application prospect.

The methods for identifying parameters and the equivalent circuit of LIB are described in Section 2. The SRCKF algorithm is put forward in Section 3. In Section 4, the details of the experiments are presented. Section 5 presents the temperature correction rules for off-line parameter identification. In Section 6, three experiments are done with both the battery cell and pack used in actual cars to prove the efficiency of the proposed method. Section 7 makes the conclusions.

2 LIB model and parameters identification

In the literature,[32] several battery models of different orders including the first-order RC model were compared, and the calculation accuracy of the model under different operating conditions is compared with the same algorithm. The first-order RC model has a good balance of

calculation accuracy, data quantity for parameter identification and calculation complexity for applying a Kalman filter. In this paper, the computational complexity, parameter identification effort and accuracy are the main considerations. Therefore, the model shown in Fig. 1 is selected for its balance of the computational complexity and accuracy in the work. U_{ocv} is the voltage of the open circuit, the terminal voltage is represented by U_t, U_p denotes the RC network polarization voltage, and R_0 stands for the battery internal resistance. The RC network consists of the polarization capacitance (C_p) and polarization resistance (R_p). C_p and R_p describe the battery transient characteristics.

After analysing the circuit, the following formulas can be written:

$$\dot{U}_p = -U_p / \left(C_p R_p\right) + i / C_p \tag{1}$$

$$U_t = U_{ocv} - U_p - U_0 \tag{2}$$

$$U_0 = I_l R_0 \tag{3}$$

Based on the principle of current integration and the RC network, the dynamics of SOC and polarization voltage can be expressed as:

$$SoC(t) = SoC(t_0) + (\eta \int_{t_0}^{t} i(t)dt) / C_N \tag{4}$$

$$U_{p,k} = \left(1 - T_s / \left(C_p R_p\right)\right) U_{p,k-1} + T_s / C_p I_{k-1} \tag{5}$$

The transfer functions can be acquired according to the RC model structure. The principles of parameter identification are to input an excitation to the battery system and to collect the corresponding response signals. With sufficient incentive and response information, the values of each parameter in the transfer function can be obtained through the iterative or fitting methods. The parameters can be identified off-line by the HPPC test using the "FreedomCAR battery test manual".[33]

A capacity test at a certain temperature is conducted to identify off-line parameters. The

temperature test is started with SOC=0.95 to perform an HPPC test cycle. The battery is then discharged until the SOC is reduced by 0.05. Another HPPC test cycle is conducted, and the cycle continues until the SOC is reduced to 0.05. The discharge test is also similar. Leveraging the HPPC testing data, the SOC dependence of both the OCV and model parameters can be determined.[32]

3 Experimental configuration and influence of temperature on battery parameters

3.1 Experimental configuration

For the cell level, a testing bench (CellBench) was built, including battery cells, equipment for charging and discharging (NBT BTS5200C4), monitoring platform, environmental box, and the hardware of the BMS and cables. It can not only perform the tests of HPPC for identifying the cell parameters off-line but also the simulation and verification under actual conditions.

For the pack level, we build a test bench (PackBench), including a battery pack, charging and discharging equipment (Chroma Model 17030), a platform for monitoring, an environmental oven, a cable for testing, and a communication cable. The functions of this test bench are the same as those of the CellBench.

The specifications of the cell and NBT BTS5200C4 are given in Tables 1 and 2, respectively. Figs. 2 and 3 show the cell level and pack level test benches, respectively.

Tables 3 and 4 are the specifications of the battery pack and the test equipment specification, respectively.

3.2 Influence of temperature on battery parameters

The temperature has a different influence on the parameters of the selected model.[26] In general, we must carry out HPPC tests at different temperatures, which ensures the SOC

estimation accuracy of the vehicle BMS at various temperatures. Conventionally a complete HPPC cycle test is performed every three or five degrees Celsius (℃) in order to identify the battery parameters at each specific temperature. According to the HPPC test cycle, in the entire temperature range, the test takes 1740 (116× (55-(-20)) /5=1740) hours, and each cycle takes approximately 116 ((16+4+8+10+20) ×2=116) hours. Therefore, a great amount of data is generated, and the whole offline test is time-consuming and expensive. It is also impossible to store so much off-line data due to the limited ROM of the embedded MCU. Therefore, it is meaningful to study efficient rules that can describe the impact of temperature on the parameters of the selected model. At the temperatures of -5 and -10 ℃, the HPPC test for LIB is performed using the HPPC test method and offline parameter identification was performed.

Fig. 4(a) and (b) compare the terminal voltage tested at -5 ℃ with the voltage simulation using off-line identification parameters at -5 and 0 ℃, respectively. Similarly, Fig. 4(c) and (d) compare the terminal voltage tested at -10℃ with the voltage simulation using off-line identification parameters at -10 ℃ and -5 ℃. The precision of SOC estimation can be greatly impacted by the temperature. Therefore, temperature compensation must be performed for both model parameters and estimation algorithms in practical applications.

4 SRCKF algorithm and temperature correction rules in off-line parameter identification

4.1 SRCKF algorithm

A total of 2*n* points with the same weights based on the transformation of cubature to approach the average of state variables are calculated by the SRCKF. After non-linear functions propagate these points, the acquired average and variance can attain third-order accuracy of the true value of non-linear functions. The covariance matrix square root is directly propagated and

updated in the Cholesky decomposition by the SRCKF algorithm, which ensures that it will not appear as a negative value and the filter will not diverge. SRCKF has the advantage over UKF and does not need to adjust the parameter factors as does the UKF. The state dimension determines the volume point and weight of the SRCKF and can be stored and calculated in advance. Therefore, the design and implementation of the SRCKF is simpler and can be performed smoothly by the on-board embedded MCU.[34]

n-dimensional non-linear discrete state space can be defined as follows:

$$x_k = f(x_{k-1}, u_{k-1}) + \omega_{k-1}, k = 0,1,\cdots; \quad (6)$$

$$z_k = h(x_k, u_k) + \upsilon_k, k = 0,1,\cdots. \quad (7)$$

The SRCKF is described in the three steps shown in Table 5:

After the state estimation value $\hat{x}_{k|k}$, the covariance square root of value $R_{k|k}$ can be acquired at time *k*. A new iteration then can be executed with the repetition of step 2 at time *k+1*.

By integrating Eqs. (1-5), the following state and observation equations are obtained:

$$x_k = \begin{bmatrix} U_{p,k} \\ SoC_k \end{bmatrix} = \begin{bmatrix} \left(1 - T_s / \left(C_p R_p\right)\right) & 0 \\ 0 & 1 \end{bmatrix} \begin{bmatrix} U_{p,k-1} \\ SoC_{k-1} \end{bmatrix} + \begin{bmatrix} T_s / C_p \\ \eta_k T_s / C_N \end{bmatrix} \left(I_{k-1}\right) + \begin{bmatrix} \omega_{1,k-1} \\ \omega_{2,k-2} \end{bmatrix} \quad (21)$$

$$z_k = \left(U_{t,k}\right) = \begin{bmatrix} 1 \\ 0 \end{bmatrix}^T \begin{bmatrix} U_{P,k} \\ SoC_k \end{bmatrix} + \left(R_0\right)\left(I_{lk}\right) + U_{OCV} + \left(\nu_k\right) \quad (22)$$

4.2 Temperature correction rules

After the HPPC test of the battery cells at various temperatures, the parameters of the model can be identified with the method described in the literature.[32]

Fig. 5 (a) presents the relationship between SOC and R_p at different temperatures (lower temperatures); Fig. 5 (b) describes the ratio of R_p with other temperatures compared to R_p at 25 ℃. Similarly, Fig. 5 (c) and (d) depict the absolute and relative values (compared with 25 ℃)

of R_0 at different SOCs. These indicate that the R_0 of battery is clearly impacted by the temperature in the low temperature zone. At the same time, in the case of SOC < 0.3, the effect of temperature is also greater on the R_p.

Fig. 6 outlines the variation of R_p and R_0 identified at different temperatures (higher temperatures), where Fig. 6(a) depicts the relationship between S OC and R_p at different temperatures (higher temperatures) and Fig. 6(b) depicts the ratio of R_p at different temperatures to that at 25 ℃. Similarly, Fig. 6 (c) and (d) describe the absolute and relative values (compared with 25 ℃) of R_0, respectively, at different SOCs. These figures show that in the high temperature zone, the R_p of the battery is not sensitive to the temperature, and the temperature is significant for the R_0.

Fig. 7(a) depicts the relationship between SOC and τ at different temperatures, and Fig. 7(b) describes the ratio of τ with other temperatures compared to τ at 25 ℃. It can be seen from the above test results that the influence of temperature on R_p and R_0 in the high temperature zone (5 ℃<T<55 ℃) is weak, especially in the range (10 ℃<T<55 ℃). The effects of temperature on R_p and R_0 are very significant in the low-temperature range (-20 ℃<T<-5 ℃). More importantly, the influence of R_0 directly causes a significant decrease in the charge and discharge performance of batteries.

From the study of the influence of temperature on battery parameters, it is known that the battery equivalent circuit model (ECM) does not work very well for the actual performance of battery voltage, which is the key factor for SOC estimation at lower ambient temperatures. However, the ECM would improve the performance of simulating battery voltage when the model parameters change the temperature status. Based on the above temperature influence law, we introduce an adjustment factor in the observation equation of the selected model when we

design the algorithm for SOC estimation. This factor describes the temperature influence on the properties of the battery. Then, a new observation formula becomes:

$$z_k = \left(U_{t,k}\right) = \begin{bmatrix} 1 \\ 0 \end{bmatrix}^T \begin{bmatrix} U_{P,k} \\ SoC_k \end{bmatrix} + \left(R_0\right)\left(I_{lk}\right) + U_{OCV} + \left(v_k\right) + u_T \tag{23}$$

In the formula, u_T represents a non-linear function of temperature. It is known from the battery cell tests that u_T tends to 0 when the temperature is greater than 5 ℃, and the influence of u_T on the observation equation increases as the temperature decreases. Fig. 8 depicts the relationship between u_T and temperature for the investigated cells. It should be noted that the temperature-dependent u_T does not change the overall structure of the state-space equation; however, it indirectly affects the state estimation through the adjustment of the system measurement. Therefore, the optimized observation equation has a strong portability, and the "model drift" under low temperature conditions can be overcome only by updating the observation equation in the original estimation model.

By analysing the changes in battery parameters at high and low temperatures, we find that the sensitivity of R_0 to temperature changes is significantly higher than to the other parameters. Although R_p also shows a certain dependence on temperature, this dependence is more pronounced in areas with temperatures below 0 ℃ and an SOC below 0.3. In contrast, C_p has high temperature dependence, considering the significance of its influence on the battery terminal voltage and its influence on SOC estimation. Therefore, the C_p should not be regarded as a major correction target of model parameters. We separately compensate the R_0, R_p, C_p and OCV, and thus their impacts on SOC estimation are obtained at different temperatures as shown in Fig. 9.

In Fig. 9 (a), it is seen that the temperature has a significant effect on R_0. At different temperatures, the modification of R_0 can significantly improve the SOC estimation accuracy. In

Fig. 9 (b), at low temperature and low SOC, the influence of R_p on the SOC estimation error also increases significantly. Therefore, we propose a two-stage correction method that only performs linear correction for R_0 in the region of high temperature and increases the R_p correction factor in the region of low temperature with lower SOC. After simplification, u_T is only linearly related to R_0, and the low-temperature region is approximately linearly related to R_p.

Through the above analysis, the calibration for R_0 can be determined by testing at the three temperature points of -20, 5 and 25 degrees Celsius. In addition, we must perform the tests at the five temperature points of -20, -15, -10, -5 and 5 degrees Celsius within the range of SOC<0.4, and the R_p correction curve is obtained after the linear fitting of R_p. Therefore, a complete HPPC test is required at only the three temperature points of -20, 5 and 25 degrees Celsius, and then the partial HPPC test is performed at SOC<0.4 at the five temperature points of -20, -15, -10, -5 and 5 degrees Celsius, thus obtaining the off-line parameters to analyse the effect of temperature.

4.3 Flow-process diagram of the proposed approach

By using the proposed method, we only need to store the parameter data identified by the HPPC test at 25 ℃ under different SOHs. For further reducing the quantity of data, R_p, R_0, C_p, OCV and SOC relations are approximated with the 6th-order polynomial fitting, and only the fitting coefficients need to be stored. This significantly reduces the data to be stored in the MCU. Fig. 10 shows the flow-process diagram of the proposed approach.

5 Results and discussion

Freescale's MPC5604B was used as an embedded MCU with the C codes converted from MATLAB's RTW tool. After that, using the Codewarrior compiler, the target machine code size was 189.3 kilobytes, which is much less than the 1000 kilobyte ROM of the MPC5604B.

To further verify whether the proposed method satisfies the actual requirements of the BMS based on the MPC5604B embedded MCU, we carried out the following experiments on the CellBench (including SRCKF and other common estimation algorithms): (1) an average calculation load rate test of the embedded MCU, (2) a performance test of the algorithm under constant current conditions for the battery cell, and the test of using the temperature correction method, and (3) under dynamic stress test (DST) conditions, a performance test with different measurement interference for the battery cell. In addition, the integration code was set for every 100 ms in the program, and the bus frequency of the MPC5604B was set to 50.0 MHz to allow the execution of computationally expensive UKF.

In general, the BMS manages the battery pack composed of multiple battery cells, so the test on the battery pack is better capable of verifying the performance of the algorithm in practice. The actual car battery pack is used on the PackBench and the new European driving cycle (NEDC) conditions with brake energy recovery is adopted. The scenarios with and without measurement interference are further analysed. Since the battery pack is an actual product from the real vehicle and only the SRCKF is implemented for SOC estimation, we set the implementation code to execute the integration code every 10 ms in the test, and the bus frequency of the MPC5604B was set to 50.0 MHz.

5.1 Experiment 1: computing cost test

To verify the computational cost of the method, a test was done to compare the SRCKF with EKF, UKF, and CKF, Table 6 showed the results. The conclusion can be done that the computing cost of SRKCF algorithm is moderate and the requirements of the SRKCF algorithm can well be satisfied with the MPC5604B embedded MCU. Moreover, the SRCKF algorithm converges to the actual SOC within 2.5 s at an initialization error of 50%.

5.2 Experiment 2: constant discharge current test with temperature correction

The cell was discharged from SOC = 1 to 0.00027 using CellBench with a constant current of 34.95 A. Fig. 11 (a) shows the constant discharge current test, while Fig. 11 (b) shows the estimation results with and without temperature correction at -5 ℃. The maximum error of SOC reaches 0.4 when the parameters are not modified. However, the maximum error is reduced to 0.04 when the temperature correction rule is considered in this work. The performances of UKF, EKF, SRCKF and CKF are shown in Table 7. The results show that the convergence speed, the average error and root mean square error (RMSE) of the SRCKF algorithm are the best compared with those of the other three algorithms. Fig. 12 (a)-(d) show the results with different approaches, and the errors of the corresponding results are shown in Fig. 12 (e)-(h). The conclusions of this experiment can be stated as follows. (1) The SRCKF has the fastest convergence and the best estimation accuracy. (2) The estimation of SRCKF is confined to a small error bounded at approximately 0 with the best stability. (3) The temperature correction rule works well. (4) The proposed method can meet the requirement of the constant current discharge condition.

5.3 Experiment 3: test using DST conditions with measuring noise

On the actual vehicle, the sensor and the collecting circuits are disrupted by interferences, causing measurement errors on the current and voltage. According to the results of actual vehicle tracking, the maximum measurement error on the current and voltage is as high as 2% in a strong jamming environment. The SOC estimation algorithm thereby must have good anti-interference characteristics. In general, the measurement noise is superimposed near the real value. To quantify the noise interference, we use the following formula to apply the interference to the current and the voltage.

$$\theta = \alpha N_{\max} / 3 \quad (27)$$

where θ is the root mean square (RMS) value of the noise, α is a scaling factor and N_{max} is the max value of current or voltage. In this paper, the situations when α=1%, 2.5%, 5% are studied. The experiment was implemented on CellBench. At 5 ℃ and actual initial SOC=0.998, the SOC of the cell changed to 0.272 after 20 DST cycles. Fig. 13 shows the voltage and current profiles for the 20 DST operating conditions with 1%, 2.5%, and 5% measurement noise added. The experimental results with the different amounts of noise added are shown in Fig. 14. It is shown that EKF, UKF and CKF have the problem of filter termination due to divergence when the noise is 1%. However, the SRCKF algorithm can work well up to 5% measurement noise. Fig. 15 shows the distribution of the estimated SOC error for the SRCKF under three different noise disturbances. Table 8 shows the performance of the SRCKF algorithm under three different levels of measurement interferences. It is concluded that the SRCKF is not sensitive to corruption by noise. Therefore, the proposed SRCKF with higher estimation accuracy in the presence of strong interferences has a great potential in practical application.

5.4 Experiment 4: battery pack test using NEDC with measuring noise (1%)

The NEDC conditions include dramatic changes in load current and voltage, which represent a typical strongly nonlinear working condition. The NEDC is very significant for validating the convergence, robustness, and accuracy of the proposed method under such tough environments. Moreover, the BMSs are often subject to unexpected noises of voltage or current sensor in an actual vehicle environment, which potentially decreases the performance of model-based observers. Therefore, the noise immunity of the proposed method is also scrutinized in this section. The PackBench using the battery pack demonstrated in Table 4 is also tested for the NEDC of the battery pack.

At 5 ℃, SOH=0.9 and actual initial SOC=0.6, Figs. 16 and 17 show the changes in the parameters of the LIB pack for the NEDC test during the test without measuring noise and with measuring noise (1%), respectively. Fig. 18 shows the experimental results of SOC estimation at 5 ℃ under various conditions, while Fig. 19 shows the corresponding error distributions.

The results show that the SRCKF algorithm can rapidly converge (approximate 2.5 s) in the NEDC experiment. With modification of the identified battery parameters at 25 ℃, the RMSE of the proposed method of the entire test is 0.42%, and even with 1% current and voltage measurement disturbances, the RMSE of the proposed method can be as high as 0.679%.

6 Conclusions

A new method for model-based SOC estimation that is applicable to embedded MCUs is presented in this paper, with particular emphasis on solving the effects of temperature. Regarding the amount of HPPC tests and the number of the parameters that need to be written in an embedded MCU, a temperature correction rule is proposed in the work. A conclusion can be done that the method proposed in the paper occupies less ROM space (189.3 kilobytes) than the MPC5604B (1000 kilobytes) with the experimental results. Moreover, the SRCKF, UKF, EKF and CKF are compiled and evaluated with the experiments. The experimental results in an actual BMS environment show that the proposed approach has a faster convergence and higher accuracy with a low load rate of 68.3%. The new method can withstand 5% noise and provide a high estimation precision. Based on the results, it is clearly indicated that the proposed square root cubature Kalman filter (SRCKF) with a temperature correction rule has great potential in its application to real vehicles where the embedded MCU is used as the main processor of the BMS.

Acknowledgements

Part of the research work was completed with the assistance of Wuhan University of Technology. The authors thanks for their contribution.

Funding

The Project was supported by China National Foundation (Grant No. 51621004). The China 863 Program sponsors this work.

References

1. Wu Y, Wang W, Ming J, Li M, Xie L, He X, et al. An Exploration of New Energy Storage System: High Energy Density, High Safety, and Fast Charging Lithium Ion Battery. *Adv Funct Mater*. 2018:1805978.
2. Kim H, Jung S. Battery hybridization for achieving both high power and high energy densities. *Int J Energy Res*. 2018;42:4383-94.
3. TAKAMI, Norio, INAGAKI, Hiroki, TATEBAYASHI, Yoshinao, et al. High-power and long-life lithium-ion batteries using lithium titanium oxide anode for automotive and stationary power applications. *J Power Sources*. 2013;244:469-75.
4. Zou C, Zhang L, Hu X, Wang Z, Wik T, Pecht M. A review of fractional-order techniques applied to lithium-ion batteries, lead-acid batteries, and supercapacitors. *J Power Sources*. 2018;390:286-96.
5. Liu X, He Y, Zheng X, Zhang J, Zeng G. A new state-of-charge estimation method for electric vehicle lithium-ion batteries based on multiple input parameter fitting model. *Int J Energy Res*. 2017;41:1265-76.
6. Fazli Khalaf A, Wang Y. Economic and environmental evaluations of dedicated and residential electric tariffs for plug-in electric vehicles. *Int J Energy Res*. 2018;42:542-58.
7. Farhad S, Nazari A. Introducing the energy efficiency map of lithium-ion batteries. *Int J Energy Res*. 2018;43:1-14.
8. Jin N, Danilov DL, Van den Hof PMJ, Donkers MCF. Parameter estimation of an electrochemistry-based lithium-ion battery model using a two-step procedure and a

parameter sensitivity analysis. *Int J Energy Res*. 2018;42:2417-30.

9. Zhang Y, Song W, Lin S, Feng Z. A novel model of the initial state of charge estimation for LiFePO4 batteries. *J Power Sources*. 2014;248:1028-33.

10. Affanni A, Bellini A, Concari C, Franceschini G, Lorenzani E, Tassoni C. EV battery state of charge: neural network based estimation. Electric Machines and Drives Conference, 2003 IEMDC'03 IEEE International. 2003;2:684-8 vol.2.

11. Hu JN, Hu JJ, Lin HB, Li XP, Jiang CL, Qiu XH, et al. State-of-charge estimation for battery management system using optimized support vector machine for regression. *J Power Sources*. 2014;269:682-93.

12. Xu J, Mi CC, Cao B, Deng J, Chen Z, Li S. The State of Charge Estimation of Lithium-Ion Batteries Based on a Proportional-Integral Observer. *IEEE Transactions on Vehicular Technology*. 2014;63:1614-21.

13. Rui X, Sun F, Zheng C, He H. A data-driven multi-scale extended Kalman filtering based parameter and state estimation approach of lithium-ion olymer battery in electric vehicles. *Appl Energy*. 2014;113:463-76.

14. Wang T, Chen S, Ren H, Zhao Y. Model-based unscented Kalman filter observer design for lithium-ion battery state of charge estimation. *Int J Energy Res*. 2018;42:1603-14.

15. He Y, Liu XT, Zhang CB, Chen ZH. A new model for State-of-Charge (SOC) estimation for high-power Li-ion batteries. *Appl Energy*. 2013;101:808-14.

16. Zhang Y, Zhang C, Zhang X. State-of-charge estimation of the lithium-ion battery system with time-varying parameter for hybrid electric vehicles. *IET Control Theory &*

Applications. 2014;8:160-7.

17. Wei Z, Zhao J, Ji D, Tseng KJ. A multi-timescale estimator for battery state of charge and capacity dual estimation based on an online identified model. *Appl Energy*. 2017;204:1264-74.

18. Zou C, Manzie C, Nešić D, Kallapur AG. Multi-time-scale observer design for state-of-charge and state-of-health of a lithium-ion battery. *J Power Sources*. 2016;335:121-30.

19. Zhao L, Lin M, Chen Y. Least-squares based coulomb counting method and its application for state-of-charge (SOC) estimation in electric vehicles. *Int J Energy Res*. 2016;40:1389-99.

20. Wei Z, Meng S, Xiong B, Ji D, Tseng KJ. Enhanced online model identification and state of charge estimation for lithium-ion battery with a FBCRLS based observer. *Appl Energy*. 2016;181:332-41.

21. Wei Z, Zou C, Leng F, Soong BH, Tseng K-J. Online Model Identification and State-of-Charge Estimate for Lithium-Ion Battery With a Recursive Total Least Squares-Based Observer. *IEEE Transactions on Industrial Electronics*. 2018;65:1336-46.

22. Zhang Y, Huang Y, Li N, Zhao L. Embedded cubature Kalman filter with adaptive setting of free parameter. *Signal Processing*. 2015;114:112-6.

23. Li LWaLWaY. A Novel State-of-Charge Estimation Algorithm of EV Battery Based on Bilinear Interpolation. 2013 IEEE Vehicle Power and Propulsion Conference (VPPC). 2013:1-4.

24. Zou C, Hu X, Dey S, Zhang L, Tang X. Nonlinear Fractional-Order Estimator With Guaranteed Robustness and Stability for Lithium-Ion Batteries. *IEEE Transactions on Industrial Electronics*. 2018;65:5951-61.

25. Xing Y, He W, Pecht M, Tsui KL. State of charge estimation of lithium-ion batteries using the open-circuit voltage at various ambient temperatures. *Appl Energy*. 2014;113:106-15.

26. Guo YaL, Maji and Zou, Jia and Liu, Yunpeng and Kang, Jianqiang. Temperature Characteristics of Ternary-Material Lithium-Ion Battery for Vehicle Applications. SAE 2016 World Congress and Exhibition. 2016.

27. Wu W, Wu W, Qiu X, Wang S. Low-temperature reversible capacity loss and aging mechanism in lithium-ion batteries for different discharge profiles. *Int J Energy Res*. 2018;43:1-11.

28. Zhang SS, Xu K, Jow TR. The low temperature performance of Li-ion batteries. *J Power Sources*. 2003;115:137-40.

29. Liao L, Zuo P, Ma Y, Chen X, An Y, Gao Y, et al. Effects of temperature on charge/discharge behaviors of LiFePO4 cathode for Li-ion batteries. *Electrochim Acta*. 2012;60:269-73.

30. Liu X, Chen Z, Zhang C, Wu J. A novel temperature-compensated model for power Li-ion batteries with dual-particle-filter state of charge estimation. *Appl Energy*. 2014;123:263-72.

31. Cho JKaSLaB. The State of Charge estimation employing empirical parameters measurements for various temperatures. 2009 IEEE 6th International Power Electronics

and Motion Control Conference. 2009:939-44.

32. Wang Q, Wang J, Zhao P, Kang J, Yan F, Du C. Correlation between the model accuracy and model-based SOC estimation. *Electrochim Acta*. 2017;228:146-59.

33. INEEL. Freedom CAR battery test manual. INEEL 2001:6-30.

34. Cui X, Jing Z, Luo M, Guo Y, Qiao H. A New Method for State of Charge Estimation of Lithium-Ion Batteries Using Square Root Cubature Kalman Filter. *Energies*. 2018;11:209.

Table 1. The battery cell specifications

Items	Values
Rated voltage	3700 mV
Rated capacity	35000 mAh
Battery cell maximum charging current	75A
Battery cell maximum discharging current	150A

Table 2. The NBT BTS5200C4 specifications

Items	Values
Voltage measurement range	0~5 V
Measurement error of current	0.1 percent (full scale), <20 mA
Measurement error of voltage	0.1 percent (full scale), <20 mV
Measurement error of temperature	±1 ℃

Table 3. Basic properties of the ternary lithium polymer battery pack

Items	Values
Battery pack burst mode	2 parallel, 96 series
Battery pack voltage	355.2 V
Battery pack capacity	70 Ah
Battery pack maximum charging	140 A
Battery pack maximum discharging	280 A

Table 4. Parameters of the Chroma Model 17030 tester for universal batteries

Items	Values
Maximum discharging/charging current	500 A
Voltage range	19~900 V
Error (measurement of current)	0.1 percent (full scale), <20 mA
Error (measurement of voltage)	0.1 percent (full scale), <20 mV
Error (measurement of temperature)	±0.2 ℃

Table 5. Flow chart of SRCKF algorithm

Step 1. Initialization

$$\begin{cases} \hat{x}_{0|0} = E(x_0) \\ S_{0|0} = chol\left(E\left[(x_0 - \hat{x}_{0|0})(x_0 - \hat{x}_{0|0})^T\right]\right) \end{cases} \tag{8}$$

Step 2. State prediction

(1) calculate the battery state cubature points at time *k-1*:

$$X_{i,k-1|k-1} = S_{k-1|k-1}\xi_i + \hat{x}_{k-1|k-1} \qquad i = 1, 2, \cdots, 2n \tag{9}$$

(2) predict the sampling points:

$$X^*_{i,k|k-1} = f(X_{i,k-1|k-1}, u_{k-1}) \tag{10}$$

(3) predict the state:

$$\hat{x}_{k|k-1} = 1/2n \sum_{i=1}^{2n} X^*_{i,k|k-1} \tag{11}$$

(4) calculate the covariance matrix square root of the state prediction error:

$$S_{k|k-1} = qr\left(\left[\chi^*_{k|k-1} \quad S_{Q,k-1}\right]\right) \tag{12}$$

where: $Q_{k-1} = S_{Q,k-1}S^T_{Q,k-1}$, and

$$\chi^*_{k|k-1} = 1/\sqrt{2n}\left[X^*_{1,k-1} - \hat{x}_{k|k-1}, X^*_{2,k-1} - \hat{x}_{k|k-1}, \cdots, X^*_{2n,k-1} - \hat{x}_{k|k-1}\right]$$

Step 3. Filtering correction

(1) generate the cubature points according to cubature rules

$$X_{i,k|k-1} = S_{k|k-1}\xi_i + \hat{x}_{k|k-1} \tag{13}$$

(2) calculate the propagated volume points

$$Z_{i,k|k-1} = h\left(X_{i,k|k-1}, u_k\right) \tag{14}$$

(3) predict the measurement vectors

$$\hat{z}_{k|k-1} = 1/2n \sum_{i=1}^{2n} Z_{i,k|k-1} \tag{15}$$

(4) estimate the innovation covariance matrix square root

$$S_{zz,k|k-1} = qr\left(\left[Z_{k|k-1} \quad S_{R,k}\right]\right) \tag{16}$$

where: $Rk = S_{R.k}S^T_{R,k}$,and

$$Z_{k|k-1} = 1/\sqrt{2n}\left[Z_{1,k|k-1} - \hat{z}_{k|k-1}, Z_{2,k|k-1} - \hat{z}_{k|k-1}, \cdots, Z_{2n,k|k-1} - \hat{z}_{k|k-1} \right]$$

(5) calculate the cross-covariance matrix between measurement and state vector

$$P_{xz,k|k-1} = \chi_{k|k-1} Z_{k|k-1}^T \tag{17}$$

where: $\chi_{k|k-1} = 1/\sqrt{2n}\left[X_{1,k|k-1} - \hat{x}_{k|k-1}, X_{2,k|k-1} - \hat{x}_{k|k-1}, \cdots, X_{2n,k|k-1} - \hat{x}_{k|k-1} \right]$

(6) calculate Kalman gain

$$W_k = \left(P_{xz,k|k-1} / S_{zz,k|k-1}^T \right) / S_{zz,k|k-1} \tag{18}$$

(7) estimate the state

$$\hat{x}_{k|k} = \hat{x}_{k|k-1} + W_k \left(z_k - \hat{z}_{k|k-1} \right) \tag{19}$$

(8) calculate the square root matrix of the state estimation error covariance at time *k*

$$S_{k|k} = qr\left(\left[\chi_{k|k-1} - W_k Z_{k|k-1} \quad W_k S_{R,k} \right] \right). \tag{20}$$

Table 6. Computing costs of different methods

Estimation methods	EKF	UKF	CKF	SRCKF
Load rate (%)	34.8	100	58.7	68.3

Table 7. Results of experiment 2

Method	Time of convergence	Method RMSE	Method max error	Method mean error
SRCKF	25 s	0.00596	0.01305	0.00013
CKF	60 s	0.00601	0.01230	0.000078
UKF	110 s	0.00971	0.01702	-0.00265
EKF	25 s	0.01215	0.02726	0.00271

Table 8. Experimental results using the proposed method with noise

Noise	RMSE	Average error	Maximum error
1.0%	0.01085	-0.00271	0.03482
2.5%	0.01691	0.00052	0.05344
5.0%	0.02002	0.00275	0.07973

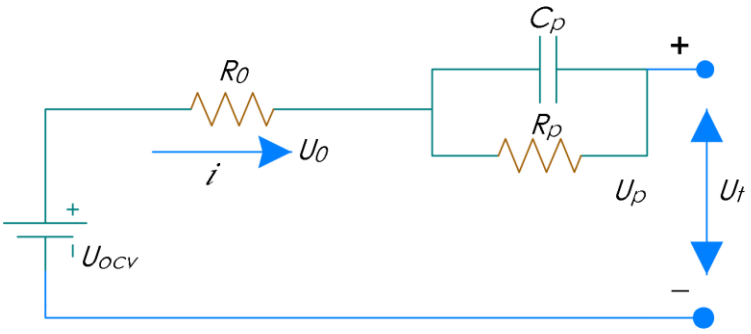

Fig. 1 The RC model of a LIB.

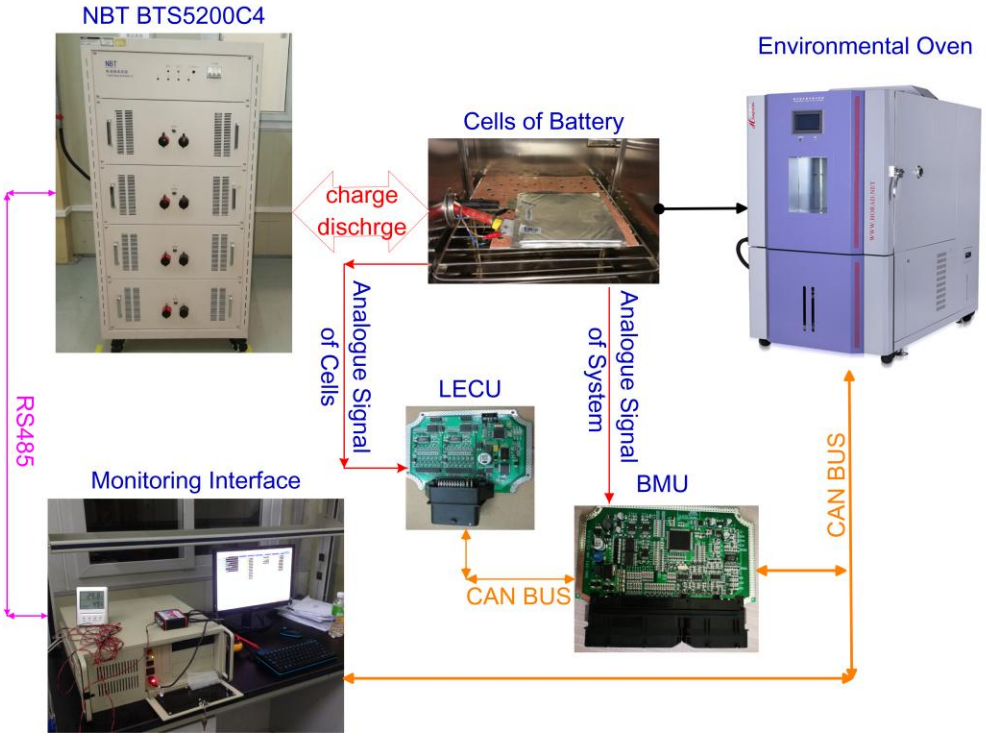

Fig. 2 Test bench for battery cell.

Fig. 3 Test bench for battery pack.

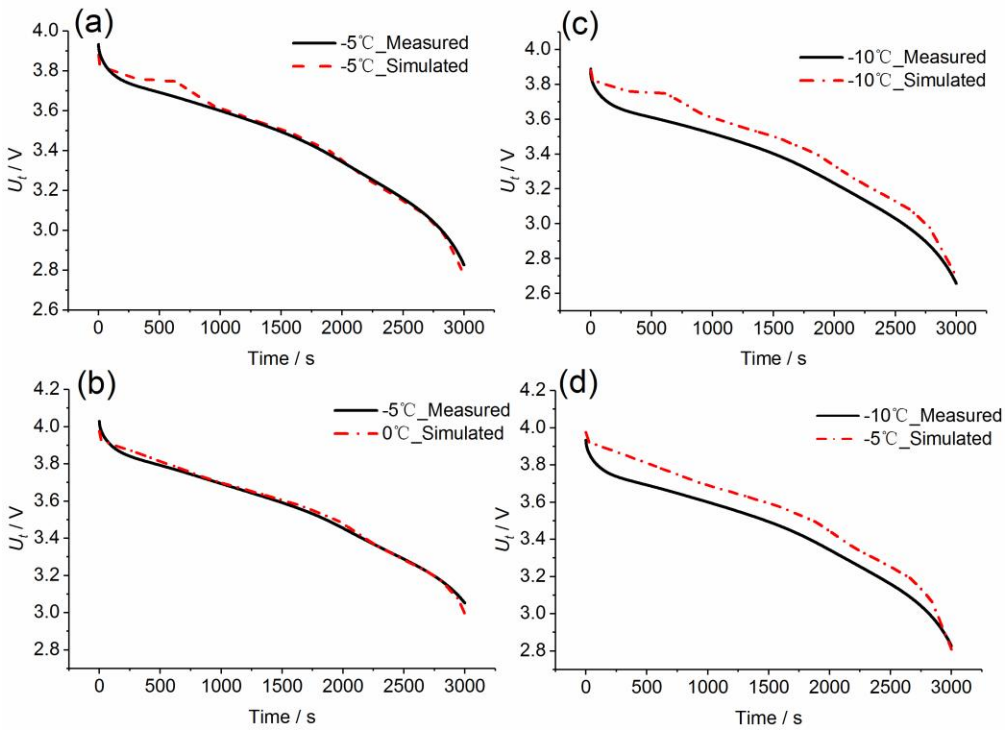

Fig. 4 The terminal voltage simulation based on the proposed model at different temperatures: (a) voltage simulation using -5 ℃ parameters, (b) voltage simulation using 0 ℃ parameters, (c) voltage simulation using -10 ℃ parameters, (d) voltage simulation using -5 ℃ parameters.

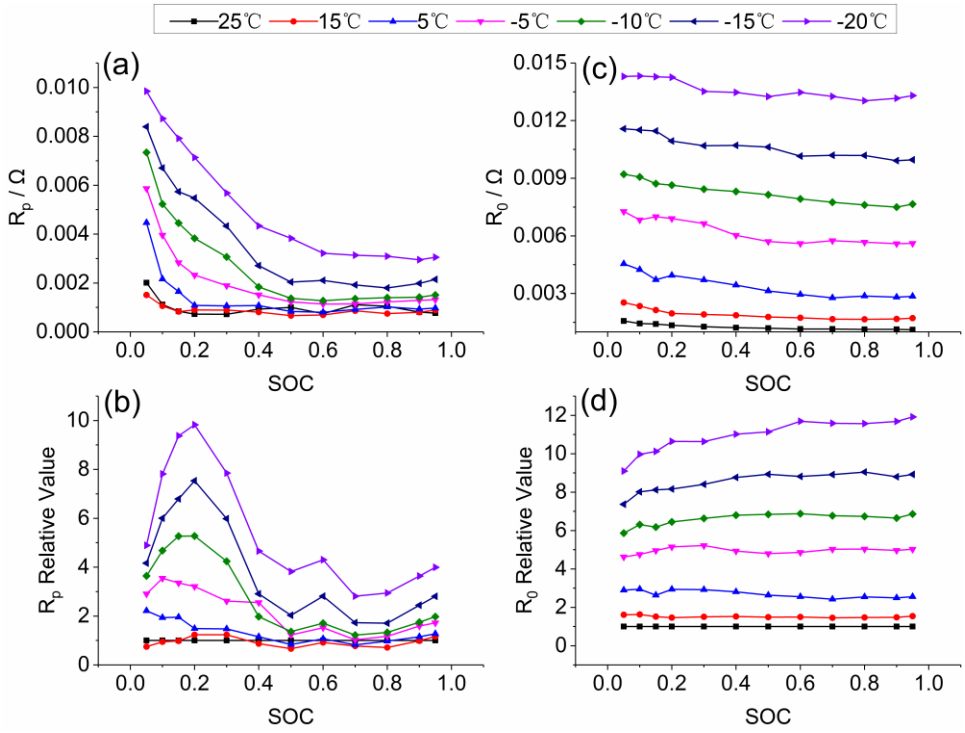

Fig. 5 Identified parameters at different temperatures (lower temperature): (a) R_p, (b) R_p relative value, (c) R_0, (d) R_0 relative value.

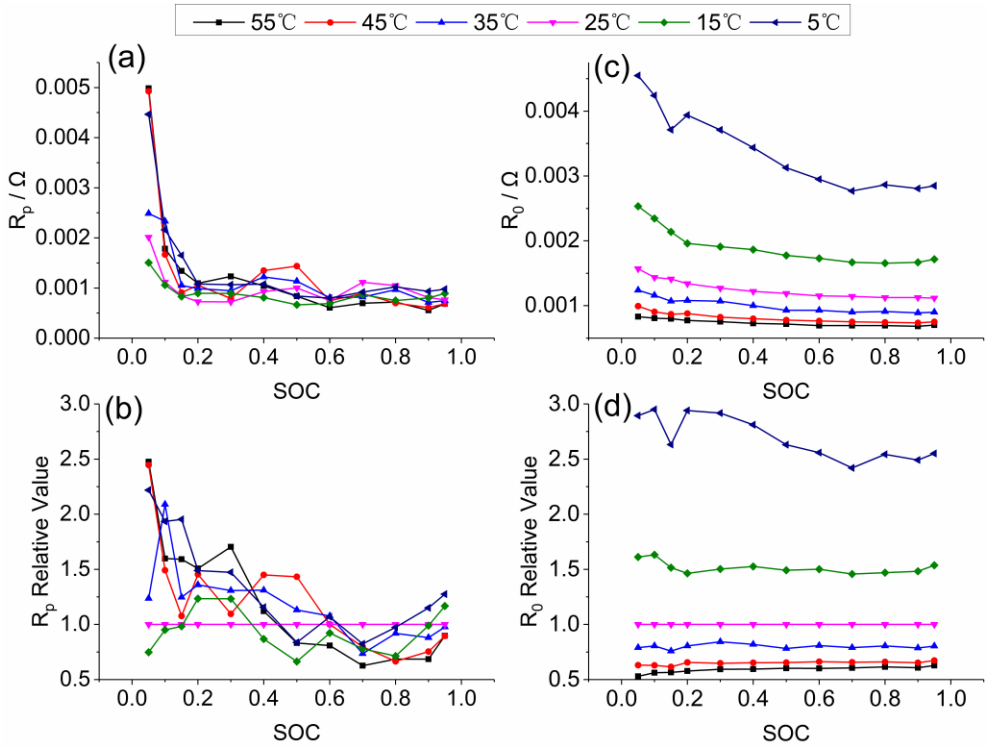

Fig. 6 Identified parameters at different temperatures (higher temperature): (a) R_p, (b) R_p relatively value, (c) R_0, (d) R_0 relatively value.

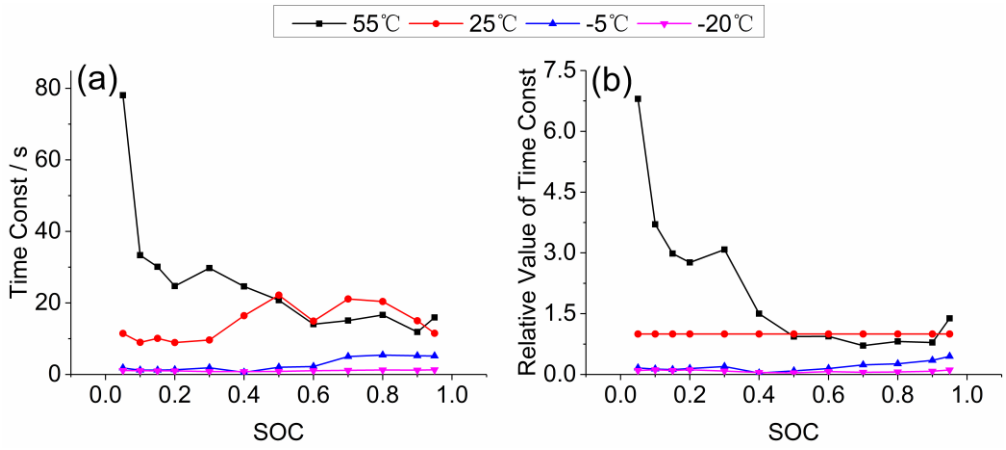

Fig. 7 Identified time constant parameters at different temperatures: (a) parameters of τ, (b) τ relative value.

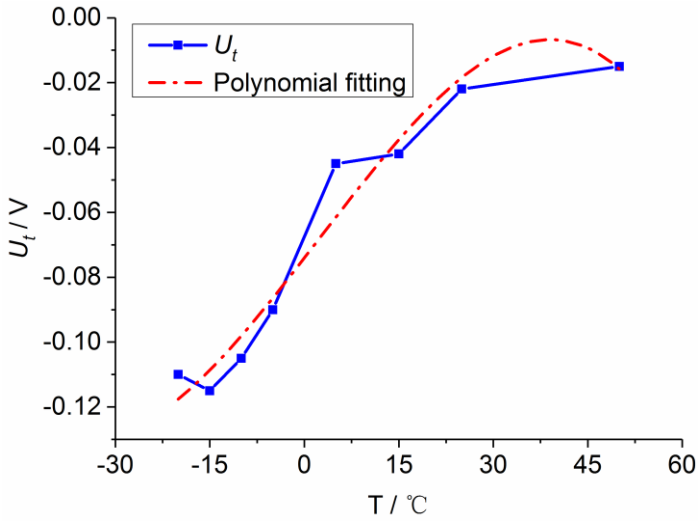

Fig. 8 Relationship between u_T and temperature for the cells.

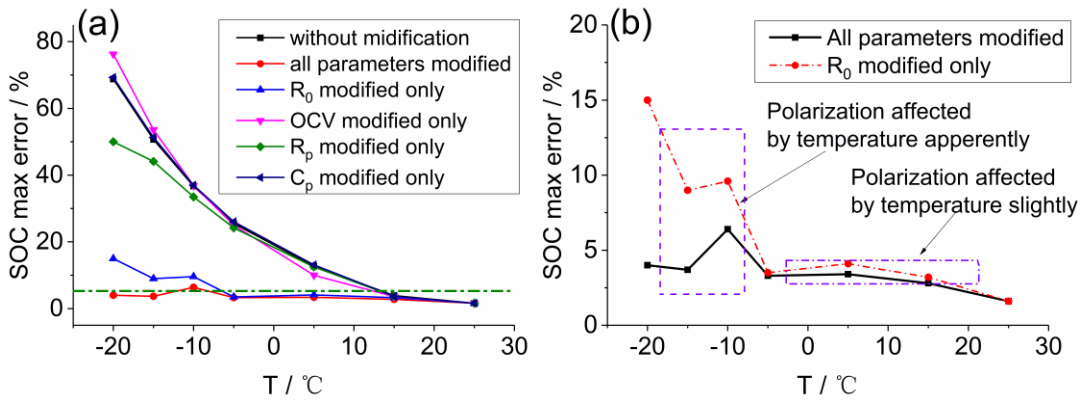

Fig. 9 Comparative results of SOC estimation influences: (a) individual parameter compensation, (b) comparative result between all parameters compensation and R_0 compensation only.

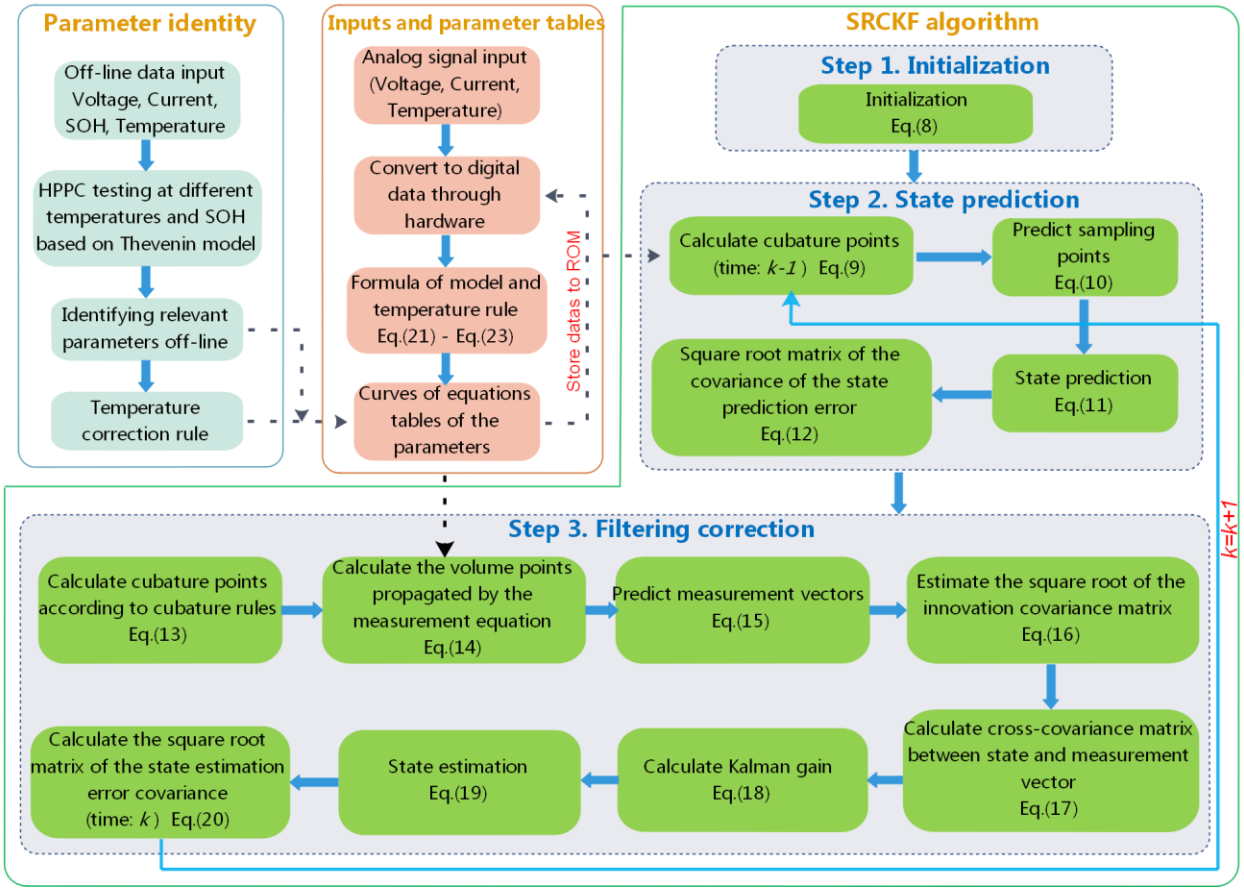

Fig. 10 SOC estimator method for the battery.

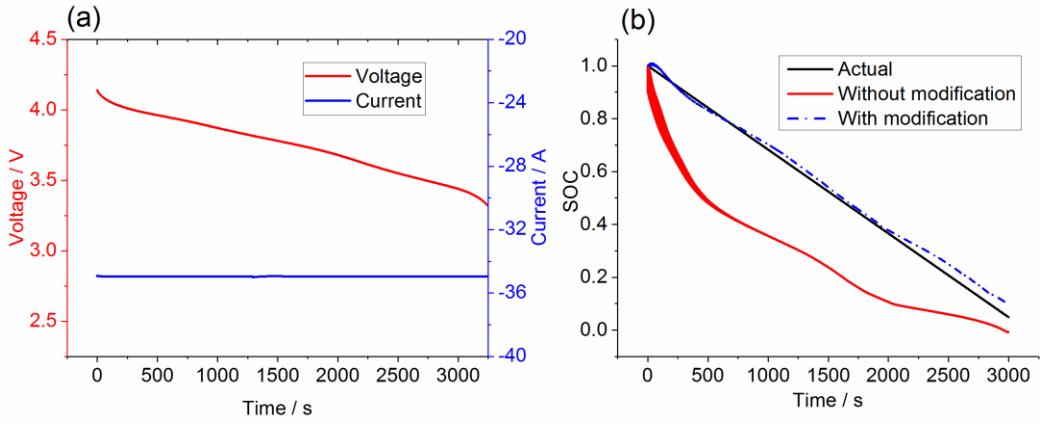

Fig. 11 (a) constant discharge current test, (b) comparison of results with and without modification.

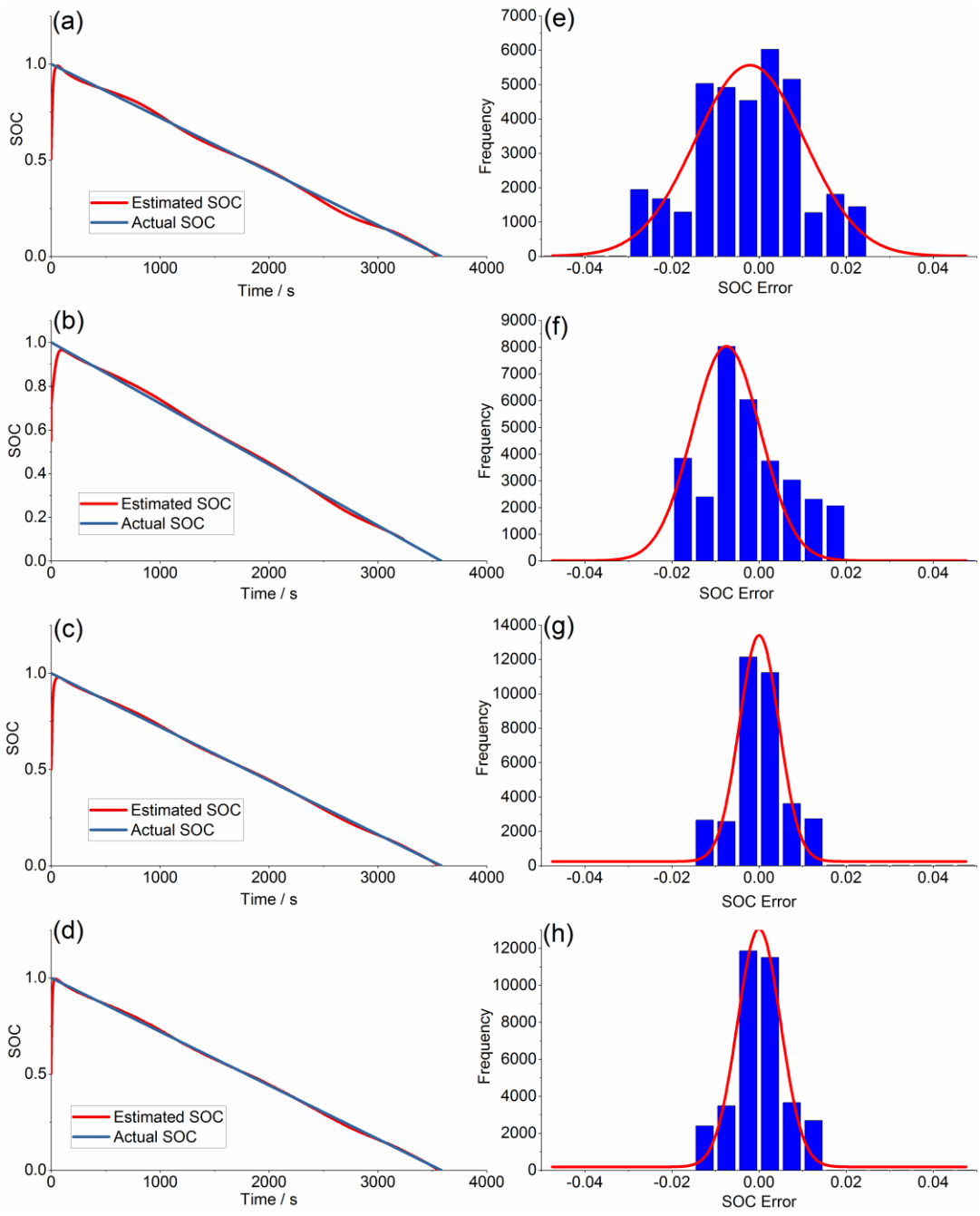

Fig. 12 The SOC results and SOC errors probability results in experiment 2: EKF for (a) (e), UKF for (b) (f), CKF for (c) (g), and SRCKF for (d) (h).

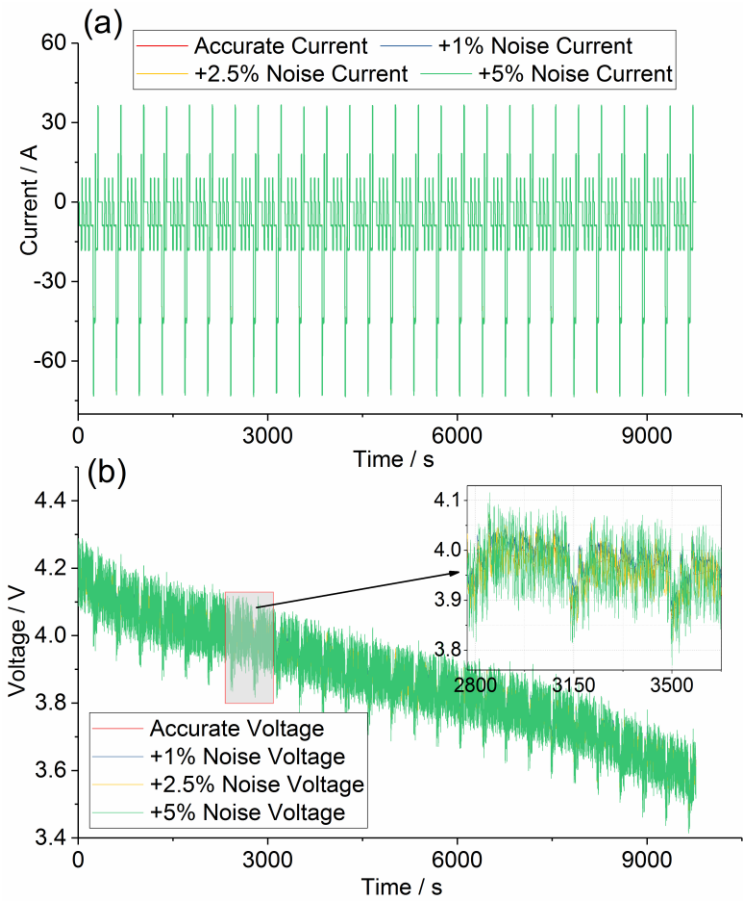

Fig. 13 Results of experiment 3 with noise: (a) DST current, (b) voltage DST.

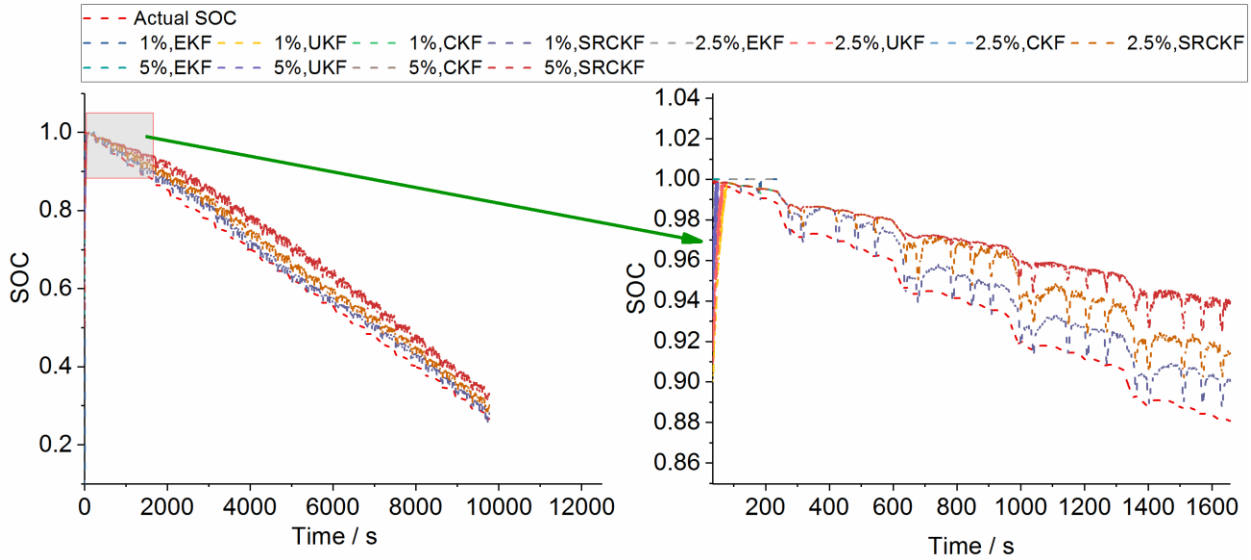

Fig. 14 Results for reckoning SOC in the DST test.

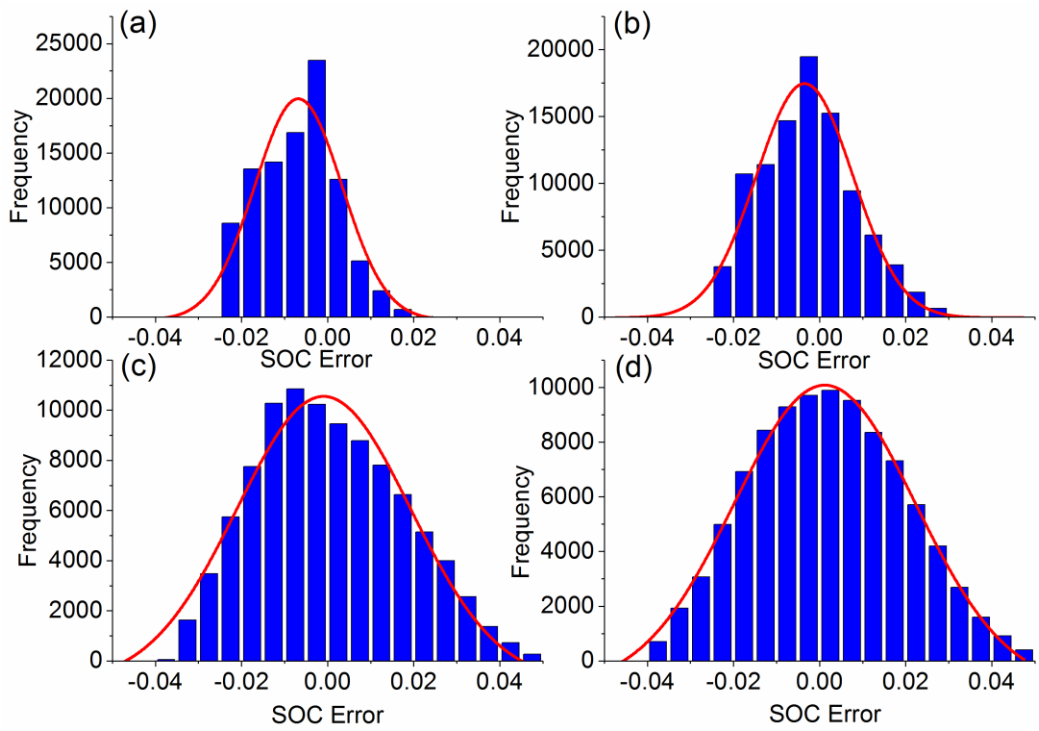

Fig. 15 Probability of SOC error in the DST test using SRCKF: (a) with 0%, (b) with 1.0%, (c) with 2.5%, (d) with 5.0%.

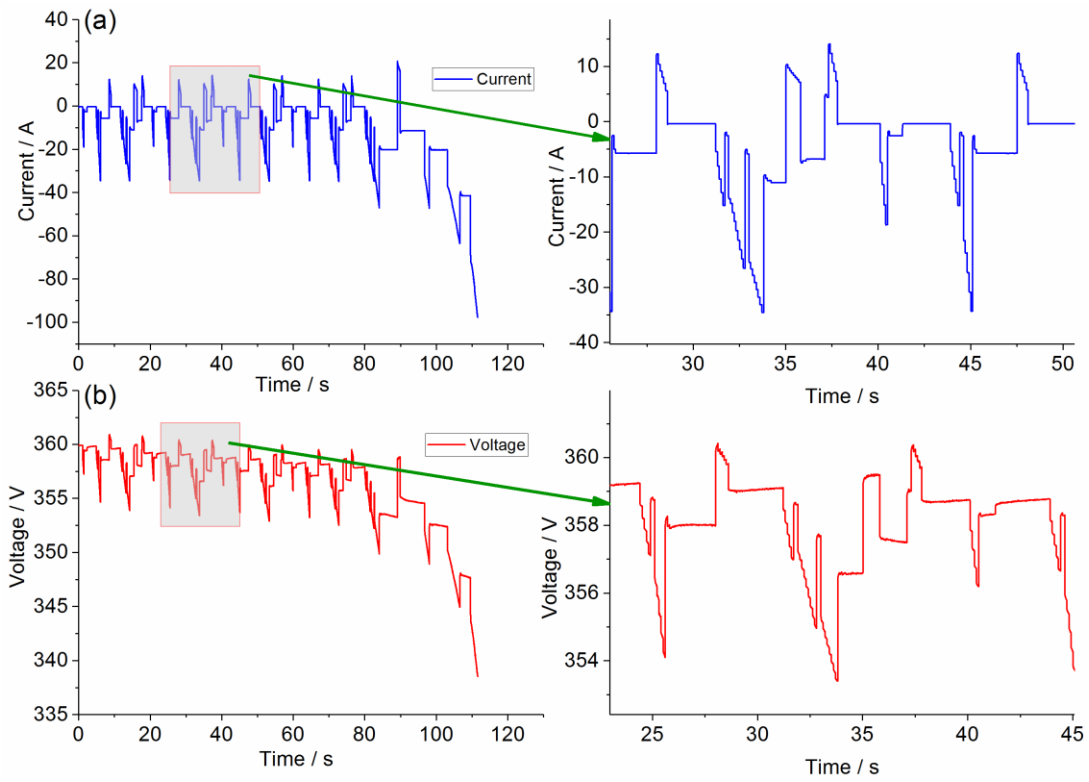

Fig. 16 Results of experiment 4 with no noise: (a) NEDC current, (b) NEDC voltage.

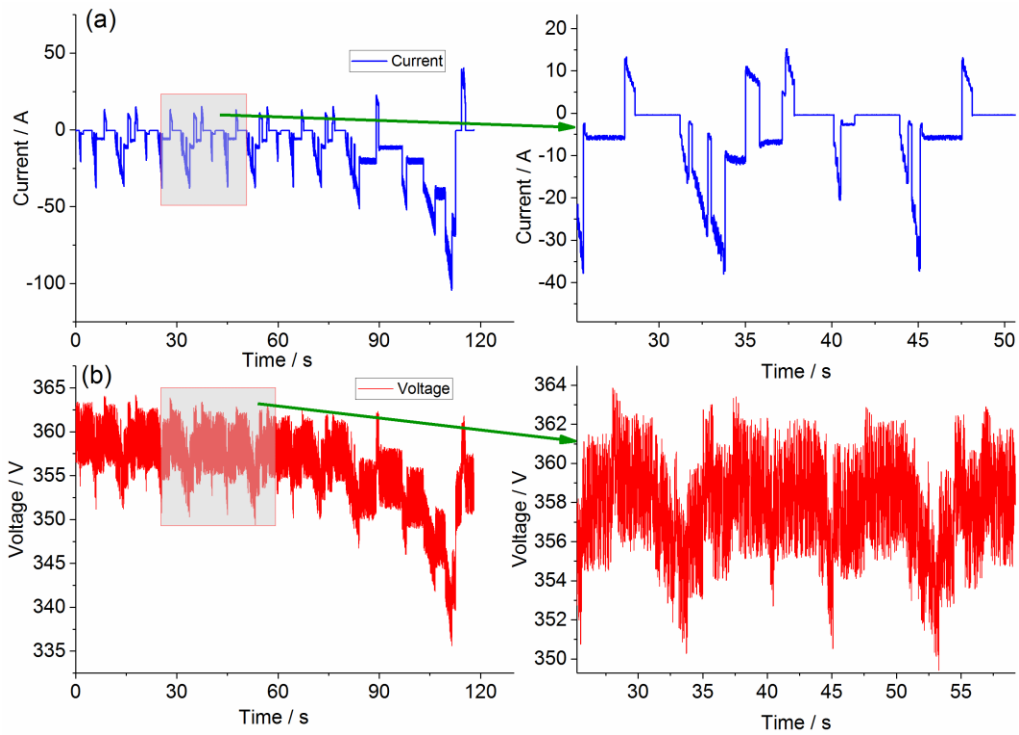

Fig. 17 Results of experiment 4 with noise (1%): (a) NEDC current, (b) NEDC voltage.

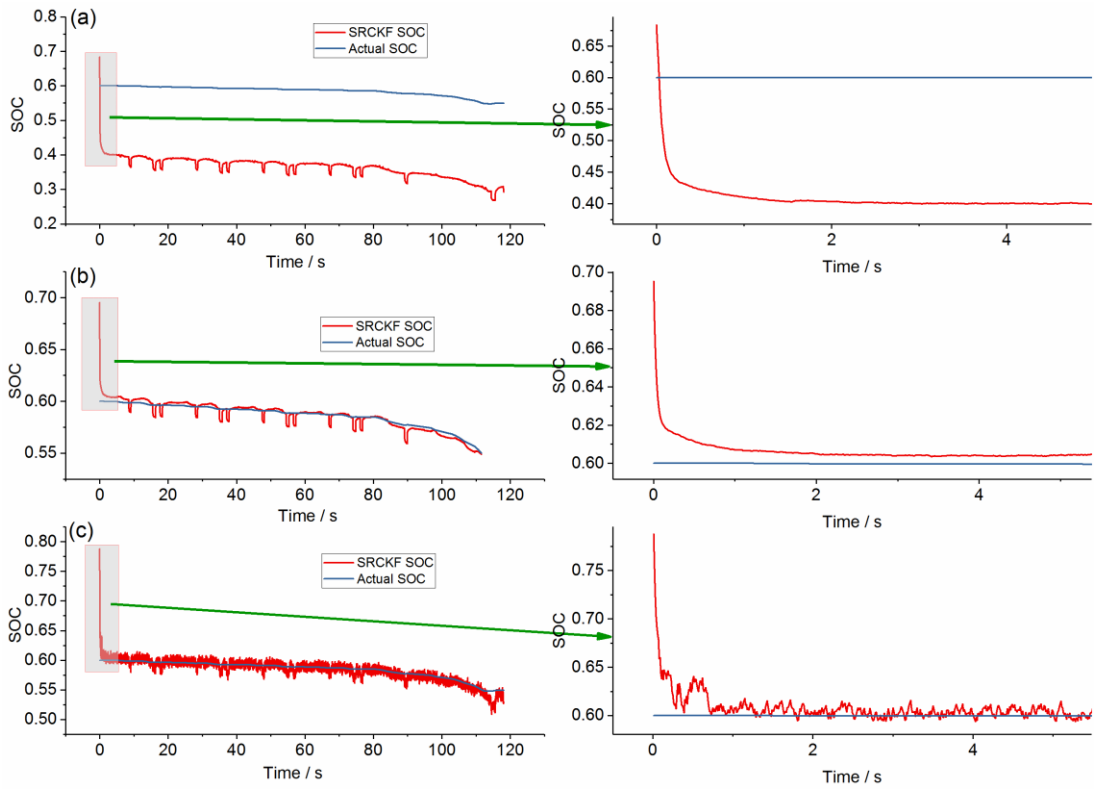

Fig. 18 Results of experiment 4: (a) no noise and using identified battery parameters at 25 ℃ without modification, (b) with modification of parameters and no noise, (c) with modification of parameters and noise (1%).

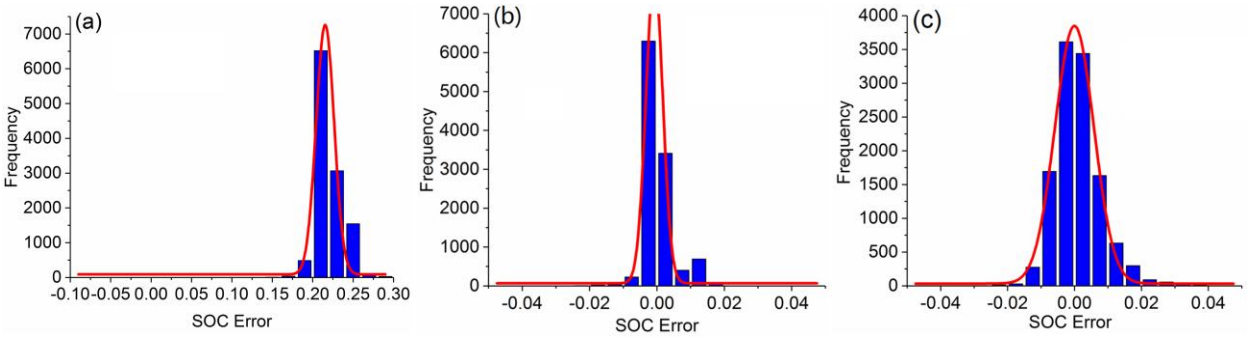

Fig. 19 Test result of distribution of the SOC estimation error: (a) with no noise without modification, (b) with no noise with modification, (c) with noise (1%).